JGR Atmospheres

RESEARCH ARTICLE
10.1029/2022JD037926

Monitoring the 2021 Cumbre Vieja Volcanic Eruption Using Satellite Multisensor Data Fusion

Elisabeth Weisz[1] **and W. Paul Menzel**[1]

[1]Space Science and Engineering Center, University of Wisconsin-Madison, Madison, WI, USA

Key Points:

- Satellite Infrared Remote Sensing provides radiance data and imagery of the Earth's atmosphere during daytime and nighttime
- Multisensor and multiplatform data fusion is applied to enhance spatial and temporal delineation of volcanic sulfur dioxide plumes
- Fusing geostationary with polar-orbiting satellite data assists monitoring volcanic eruptions to benefit aviation safety

Correspondence to:
E. Weisz,
elisabeth.weisz@ssec.wisc.edu

Citation:
Weisz, E., & Menzel, W. P. (2023). Monitoring the 2021 Cumbre Vieja volcanic eruption using satellite multisensor data fusion. *Journal of Geophysical Research: Atmospheres*, *128*, e2022JD037926. https://doi.org/10.1029/2022JD037926

Received 27 SEP 2022
Accepted 21 DEC 2022

Abstract Multisensor satellite data fusion merges measurements or products from imaging and sounding instruments with different spatial, spectral, and temporal resolution to obtain more comprehensive information about key atmospheric variables and processes. Here, data from low Earth and geostationary orbits, such as the Joint Polar Satellite Systems and Geostationary Operational Environmental Satellites platforms, respectively, are integrated using spatial-temporal fusion to enhance the detection of trace gas emissions from volcanoes. Not only does this yield trace gas information with improved spatial detail but, more importantly, the fusion product is also made available at significantly increased temporal resolution to help monitor the variable dispersion of trace gas emissions. The emission and dispersion of volcanic sulfur dioxide and ash plumes from the Cumbre Vieja volcano (Canary Islands, Spain) eruptions in October 2021 are studied through the synergistic exploitation of measurements and products from the Visible Infrared Imaging Radiometer Suite, the Cross-track Infrared Sounder, the TROPOspheric Monitoring Instrument, and the Advanced Baseline Imager. Fusion results show increased spatial and temporal detail and describe evolution and directionality of the volcanic ash plumes; the potential benefits range from improved air quality monitoring to better guidance from aircraft safety systems.

Plain Language Summary Improved delineation of volcanic emissions is shown via fusion of the high spectral resolution sounder Cross-track Infrared Sounder (CrIS) or TROPOspheric Monitoring instrument (TROPOMI), with Visible Infrared Imaging Radiometer Suite or Advanced Baseline Imager (ABI) data. Whereas ABI is onboard geostationary satellite platforms, which offer fast temporal coverage, the other instruments are on low-Earth orbit platforms providing twice daily global coverage instead. Sulfur dioxide (SO_2) and ash from the Cumbre Vieja volcano eruptions on La Palma in the Canary Islands are tracked on two separate days in October 2021. While TROPOMI, since it measures in the visible and ultraviolet spectral ranges, is limited to daytime viewing, CrIS infrared measurements offer night and day coverage of SO_2. Fusion with ABI enables the extension to time sequences of the changes in the emissions and the resulting plumes. This fusion demonstration foreshadows capabilities of planned future geostationary sensors.

1. Introduction

Volcanic eruptions emit large amounts of gas and aerosol into the atmosphere, which can have significant impact and consequences on human health (Baxter, 2005), economics, environment, and climate (Carn et al., 2021). For example, volcanic eruptions have been causing problems to aviation with emissions of ash, sulfate aerosols, and SO_2 over large distances that occur in unpredictable fashion and spread with the winds (Constantine et al., 2000; Prata, 2009; Prata & Tupper, 2009). Rerouting aircraft around volcanic emissions requires accurate and timely delineation of their location and mass. It is therefore critical to improve our scientific understanding of the underlying complex and diverse processes of volcanic eruptions in order to develop methods to accurately determine density and dispersion pattern of hazardous volcanic ash and gas plumes. Satellite-based remote sensing data and imagery are fundamental in forecasting, detecting, and tracking eruptive activity (Carn et al., 2009; Poland et al., 2020). Sulfur dioxide (SO_2) is one of the most abundant gases in volcanic emissions that can be measured by satellite-based instruments (Carn et al., 2016). Advanced high spectral resolution (or simply referred to as hyperspectral in this paper) sounders such as the Atmospheric Infrared Sounder (AIRS), the Infrared Atmospheric Sounding Interferometer (IASI), and the Cross-track Infrared Sounder (CrIS) were designed to measure the radiance emitted from the Earth system using several thousands of channels in the infrared (IR) spectral range (~3.6–15.5 μm), and to provide reliable global daytime and nighttime coverage from low-Earth orbit. These high spectral (which translates to high vertical) resolution data also encompass well-characterized SO_2 absorption lines (among other trace gas species). Especially IASI, with its continuous spectral sampling (in

Table 1
Instruments Used in the Fusion Approach and Their Relevant Characteristics Along With the Primary Variables Derived From Their Measurements

Instrument	Platform agency	Orbit	Spectral range	Spatial resolution	Temporal resolution	Primary variables
VIIRS	SNPP, NOAA-20 NOAA & NASA	LEO	412 nm–12 μm (VIS, NIR, IR, DNB)	750 m (for M-bands)	Twice daily GC	Imagery of surface and cloud properties, temperature and H_2O
CrIS	SNPP, NOAA-20 NOAA & NASA	LEO	3.92–15.4 μm (hyperspectral IR)	14 km (nadir)	Twice daily GC	Temperature and H_2O profiles, surface, cloud, and trace gas parameters
TROPOMI	Sentinel-5P ESA	LEO	270–2,385 nm (UV-VIS, NIR, SWIR)	3.5 × 5.5 km	Daily GC	Trace gas concentrations (e.g., O_3, NO_2, SO_2, CO, CH_4)
ABI	GOES-16 NOAA & NASA	GEO	0.47–13.3 μm (2 VIS, 4 NIR, 10 IR)	2 km (for bands >2 μm)	10 min (full disk)	Imagery of temperature, H_2O, O_3, SO_2, clouds

Note. GC stands for global coverage.

over IR 8,400 channels), is routinely used to provide accurate SO_2 total column and profile retrievals (Clarisse et al., 2008, 2012; Karagulian et al., 2010). Space-based sensors that are used to survey SO_2 (and other trace gases) also include ultraviolet (UV) and near-IR (NIR) sensors, such as the TROPOspheric Monitoring Instrument (TROPOMI). TROPOMI, onboard the low-Earth-orbit Sentinel-5 Precursor (S5p) platform, provides daily (daylight only) global observations of key atmospheric constituents to benefit, among others, services related to air quality and aircraft safety. This paper presents fusion of 750-m spatial resolution radiances from Visible Infrared Imaging Radiometer Suite (VIIRS), onboard the NOAA-20 (also known as JPSS-1) satellite, with 5.5 km spatial resolution TROPOMI Level 2 (L2) data yielding a fusion product at VIIRS high spatial resolution. Furthermore, to create time sequences of high spatial resolution products we also perform GEO/LEO fusion; specifically, high spatial (2 km) and high temporal (10 min) resolution GOES-16 ABI (Geostationary Operational Environmental Satellites-16 Advanced Baseline Imager) radiance data are combined with TROPOMI L2 data to obtain a fusion product at ABI spatial and temporal resolution. In the absence of a geostationary hyperspectral IR sounder, we highlight the value of using GEO/LEO fusion to transfer LEO hyperspectral sounder information content to GEO imager time and space resolution. Fusion of GOES-16 ABI with NOAA-20 CrIS data, which expands the detection of SO_2 into the nighttime, is also shown and discussed. A case study is presented for the eruption at the Cumbre Vieja volcanic ridge, comprising the southern half of the island La Palma in the Canary Islands (Spain). A recent eruption started on 19 September 2021 and ended on 13 December 2021; at 85 days it is the longest known eruption on La Palma (López & Jiménez, 2021). We selected a day of strong emission, 9 October 2021, and one of slightly lesser activity, 18 October 2021, where clear skies allowed satellite measurements of the volcanic emissions.

A brief description of the utilized satellite sensors and the data fusion methodology is provided in Sections 2.1 and 2.2, respectively. Volcanic SO_2 and ash emissions from the Cumbre Vieja volcano on 9 and 18 October 2021 are investigated through VIIRS/TROPOMI fusion in Section 3, ABI/TROPOMI fusion in Section 4, and ABI/CrIS fusion in Section 5. Section 6 summarizes the work and discusses its possible implications for improving air quality warning and aircraft safety risk assessment systems.

2. The Fusion Approach

2.1. Satellite Instrumentation and Products

Measurements and/or products from the following space-based instruments (listed in Table 1) are implemented in a fusion approach. The TROPOMI, a nadir-viewing imaging spectrometer and the sole payload onboard the Copernicus Sentinel-5 Precursor (S5p) platform (e.g., Veefkind et al., 2012), launched in 2017 in a near-polar, sun-synchronous orbit by the European Space Agency (ESA), utilizes the 270–2,385 nm (ultraviolet, visible, near, and shortwave infrared) spectral range, and delivers accurate atmospheric composition data products, for example, SO_2 and aerosol, with a ground pixel size of 5.5 km. We focus on TROPOMI SO_2 vertical column (Theys et al., 2022) and the ultraviolet Aerosol Index (AI) products (Stein Zweers, 2021), which are key data products to assess the volcanic processes, emissions, and impacts (Theys et al., 2019). The VIIRS (e.g., Hillger et al., 2013), onboard the National Oceanic and Atmospheric Administration (NOAA) operational S-NPP (Suomi-National Polar-orbiting Partnership) and NOAA-20 platforms in low-Earth orbit (LEO), offers high

spatial 750 m resolution visible (VIS), near-infrared (NIR), and infrared (IR) images of ocean, land, and atmospheric features in 16 spectral bands. On the same platforms, the CrIS (e.g., Han et al., 2013), a high spectral resolution interferometer, provides very accurate radiance measurements in more than 2,200 infrared channels (in full spectral resolution mode) which are used to provide detailed atmospheric temperature and moisture observations as well as trace gas determinations for various weather and climate applications. The CrIS field-of-view (FOV) size is approximately 14 km at nadir. In geostationary orbit (GEO) the Geostationary Operational Environmental Satellite (GOES)-R series hosts the ABI (e.g., Schmit et al., 2017). ABI provides radiance measurements and imagery of the earth with 16 bands (2 visible, 4 NIR, and 10 IR) at high spatial (0.5–2 km) and high temporal resolution (e.g., ABI default scan mode provides a full-disk image every 10 min) that are used in a wide range of applications, for example, related to severe weather and natural hazards monitoring.

2.2. Imager and Sounder Data Fusion

Given an increasing availability of advanced space-borne instruments on different platforms and orbital tracks and of different instrument designs, combined data utilization requires a robust, efficient, and reliable fusion approach. We outline one below.

2.2.1. Imager and Sounder Spatial Data Fusion

Our imager and sounder (hereafter written as imager/sounder) spatial fusion generally has two steps (Weisz et al., 2017). In the first step, imager radiance data is the input to a nearest neighbor search—specifically a multidimensional k-d tree search—to connect imager single pixel radiances with a selected number (usually five) of nearby coarser resolution imager radiances; the latter are the same imager radiances but averaged over collocated sounder fields-of-view (FOVs). The search of the imager data finds, for each imager pixel, the closest—in radiance and geometric space, where each dimension in the search has been normalized to a maximum value of one—coarser (low spatial) resolution FOVs. In other words, the first step provides the indices of the top five FOVs that are the closest in radiance and geolocation values of each imager pixel, and these selected FOVs are referred to as the closest or best matches hereafter. In the second step, the mean of the sounder data (e.g., sounder radiances convolved to a specific spectral band) at these selected FOVs is computed to provide the fusion result at an imager pixel. This method was originally developed to create new imager bands (e.g., by performing VIIRS/CrIS fusion, as described in detail by Weisz et al. (2017)), from hyperspectral sounders with the requirement of maintaining the imager high spatial resolution. This type of fusion is referred to as radiance fusion. In a follow-up paper, Weisz and Menzel (2019) extended the fusion to include products, where hyperspectral sounder retrieval products (e.g., clear-sky temperature and moisture layers, atmospheric stability indices)—instead of convolved radiance data—are averaged (within the second fusion step) to create the new sounding products at the imager's high spatial resolution. This is referred to as product fusion.

2.2.2. Temporal Data Fusion

Spatial fusion (i.e., LEO/LEO imager/sounder fusion such as VIIRS/CrIS or VIIRS/TROPOMI, as described in Section 2.2.1) can be augmented by temporal fusion when a GEO imager is considered. GEO/LEO imager/sounder temporal fusion connects data sets from two different times in a similar manner as in spatial fusion. In temporal fusion (Weisz & Menzel, 2019, 2020), the GEO/LEO imager/sounder spatial fusion results (e.g., ABI/TROPOMI or ABI/CrIS) from the LEO overpass time are transferred to earlier or subsequent GEO times. Specifically, a k-d tree search is performed on each ABI imager radiance from the next nonoverpass time to find the best matching ABI imager radiances from the overpass time, followed by computing the average of the fusion products associated with the selected radiances from the overpass time. This transfers spatial fusion results from the overpass time to the next time step. This transfer is repeated for successive time steps with the new time fusion product developed from the previous time fusion products.

2.2.3. Spatial-Temporal Fusion and Trace Gases

Spatial-temporal fusion consists of one spatial fusion step at the coincident GEO/LEO measurement/overpass time followed by multiple temporal fusion steps, which generates a final fusion product that has both increased spatial and temporal resolution. The latter is extremely relevant for trace gas detection and tracking, since most pollutants are highly variable in density, space, and time, and therefore cannot be detected in a timely manner by LEO sounders alone. Another aspect worth emphasizing is that the first fusion step (i.e., the best matching

geometric and radiometric search) is always done with only imager radiometric or Level 1 data (i.e., radiances or brightness temperature differences), either between high and low spatial resolution imager data (in spatial fusion, see Section 2.2.1) or between high spatial resolution imager data from adjacent time steps (in temporal fusion, see Section 2.2.2). The imager spectral bands used in the k-d tree search depend on the availability and the sensitivity to the retrieval parameter (e.g., moisture layers or tropospheric trace gas column). For both VIIRS and ABI fusion with TROPOMI in this work, we use the brightness temperature (BT) differences between the split-window bands (near 10.5 and 12 μm) to guide the k-d tree search with atmospheric (tropospheric) total column moisture concentrations. For ABI fusion with CrIS, we use the SO_2 sensitive 7.3 μm band (i.e., ABI band 10 or B10) so that the search is based on tropospheric SO_2 detection. Weisz and Menzel (2020) demonstrated that imager/sounder spatial-temporal fusion can generate tropospheric trace gas products (from volcanic, fire, and industrial sources) with high spatial resolution that can identify small-scale features with high temporal resolution to monitor trace gas emission rates and movement. Here we give further evidence of the capability of the fusion approach for revealing more detail, with the focus on volcanic SO_2 and ash dissemination, via three instrument pairings, namely, (a) VIIRS/TROPOMI, (b) ABI/TROPOMI, and (c) ABI/CrIS. The results shown below (Sections 3–5) were derived by using VIIRS "B15 minus B16" (10.8–12.0 μm) brightness temperature differences (BTD) for the k-d tree search in VIIRS/TROPOMI fusion, while for ABI/TROPOMI fusion the ABI " B13 minus B15" (10.3–12.3 μm) BTD search or the ABI B10 radiance search were employed. The ABI B10 radiance search was also made use of in the ABI/CrIS fusion. In ABI/TROPOMI fusion TROPOMI L2 products (SO_2 and AI) are used, and in ABI/CrIS fusion SO_2 detection is represented by the CrIS BTD of two CrIS channels (1,345 and 1,325 cm^{-1}), one sensitive to SO_2 and the other not (see Section 5 and the Appendix A).

3. VIIRS/TROPOMI Fusion Results

TROPOMI, which measures in the UV, VIS, NIR, and SWIR spectral regions, enables the estimation of the total vertical column of SO_2 and the UV Aerosol Index (AI), which are shown for 9 October 2021 over the Canary Islands in Figure 1 (top). It is noted that in Figure 1, and in every subsequent figure, data with values outside the lower color range limit are not displayed. TROPOMI AI is based on the spectral contrast for a given UV wavelength pair; in this paper we make use of the 340–380 nm wavelength pair. NOAA-20 VIIRS radiances are used in the spatial fusion approach to transfer TROPOMI L2 data (as outlined in Section 2.2.1) to the VIIRS higher spatial resolution and thus to further delineate the total vertical column of SO_2 (noted in Dobson units or DU) and AI detection. It is important to note that we use the AI as an indicator of ash near the volcanic eruption where the signal is dominated by the emitted ash, but further away in space and time other aerosols may be contributing to the AI signal.

VIIRS/TROPOMI fusion is accomplished by using the VIIRS split-window band (10.8 and 12.0 μm) radiance measurements (specifically, their BT differences) within the first fusion step. The BT difference offers sensitivity to the total column of tropospheric moisture and hence is indicative of the airmass which connects with the movement of SO_2 (see discussion in Section 5). The split-window also has direct sensitivity to volcanic ash. The five best TROPOMI FOV matches identified by the search are then averaged (in the second fusion step) to yield the high horizontal resolution TROPOMI products as shown in Figure 1 (bottom panels). The TROPOMI overpass of La Palma occurred around 15:00 UTC on 9 October 2021, whereas the NOAA-20 VIIRS granule start time is approximately 14:00 UTC. There is clear evidence of an SO_2 plume blowing to the southeast in the left panels, while the aerosol index shown in the right panels indicate overlap with the SO_2 plume near the eruption site. It is noted that TROPOMI aerosol index data also contain background noise from cloud and land surfaces, which therefore is still present in the fusion results. For both SO_2 and AI, the VIIRS/TROPOMI fusion offers a more detailed depiction.

Figure 2 shows similar results for 18 October 2021 along with a zoom in Figure 3 to highlight the additional detail accomplished with VIIRS/TROPOMI fusion. The TROPOMI overpass of La Palma occurred around 13:50 UTC on 18 October 2021, whereas the NOAA-20 VIIRS granule start time is approximately 14:30 UTC. On this day, the eruption was slightly less intense than on 9 October 2021 and the SO_2 plume is blowing to the north. Aerosol is mostly clustered near the Cumbre Vieja volcano. Again, the SO_2 plume is covering a larger area and perhaps indicating potential danger to aircraft where aerosol is undetected. Figure 3 illustrates how fusion details the pockets of high SO_2 concentration ($\leq$60 DU) within the plume background ($\sim$10 DU). The zoom of the aerosol index shows where fusion is providing more definition in the vicinity of the eruption.

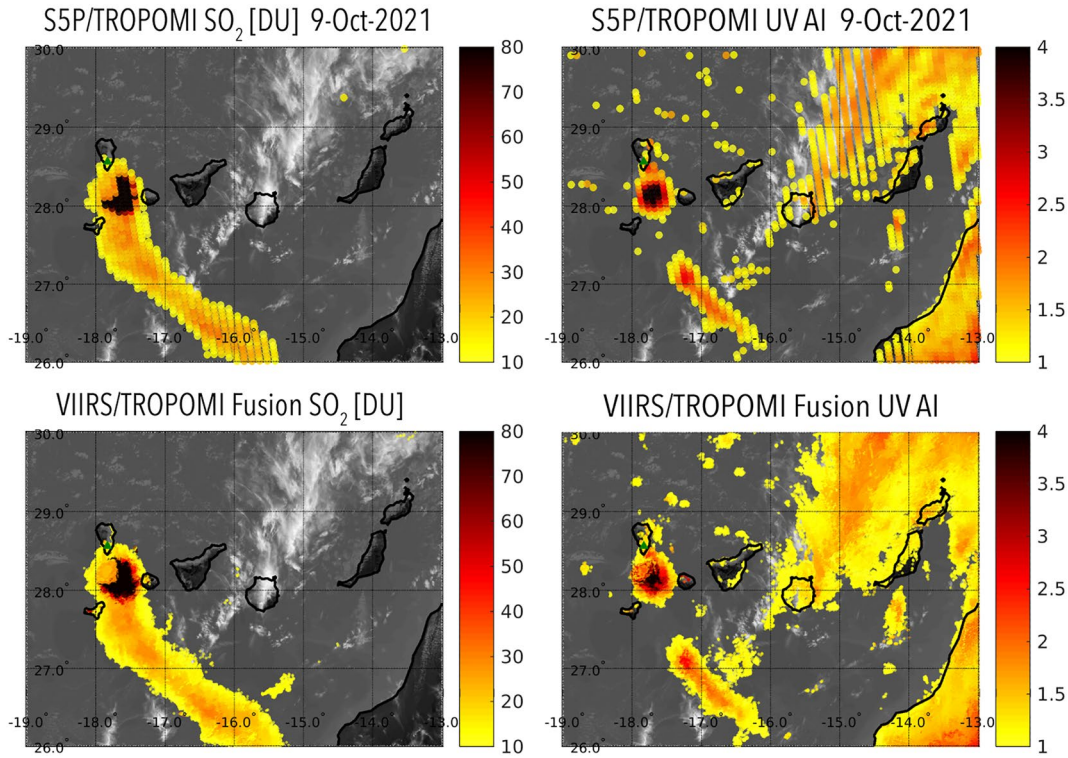

Figure 1. TROPOspheric Monitoring Instrument (TROPOMI) (top) and Visible Infrared Imaging Radiometer Suite (VIIRS)/TROPOMI fusion (bottom) of SO_2 in DU (left) and the UV AI (right), superimposed upon VIIRS Band 15 (10.8 μm) brightness temperatures for 9 October 2021. TROPOMI and NOAA-20 overpasses of La Palma occurred around 15:00 UTC and 14:00 UTC, respectively.

4. ABI/TROPOMI Fusion Results

Volcanic emission of ash and SO_2 was also investigated with a combination of LEO and GEO data in a fusion approach. GOES-16 ABI split-window infrared BT differences (at 10.35 and 12.3 μm) with 2-km spatial resolution are used in the k-d tree search. ABI/TROPOMI SO_2 and AI spatial fusion resulting from the overpass time is then transferred to 10-min temporal resolution (see Section 2.2.3) to capture the distribution changes at subsequent (or earlier) ABI measurement times. Figure 4 shows an hourly time sequence of total column SO_2 fusion images from 13:00 to 16:00 UTC on 9 October 2021 generated from the TROPOMI overpass at 15:00 UTC along with the hourly ABI true color sequence for the same times. The true color images (Miller et al., 2012) give an indication of the changes in the extent of the volcanic ash plume during the 3 hr, and the ABI/TROPOMI spatial and temporal fusion adds clearer delineation of increase in SO_2 emission at the volcano, the southward extension of the SO_2 plume, and its gradual movement to the southeast.

Airborne ash is tracked operationally by utilizing the split-window (11 and 12 μm) IR bands of geostationary satellite sensors like ABI (Pavolonis et al., 2006). Figure 5 shows a sequence of the ABI ash/dust loading product (Pavolonis & Sieglaff, 2012) for 13:30, 14:00, and 14:30 UTC on 9 October 2021 along with the ABI/TROPOMI fusion results for AI. The ABI ash/dust loading product clearly picks up the ash maximum near the volcanic source and its southward movement, but misses a secondary maximum south of the volcano and does not show a continuous plume. The ABI/TROPOMI fusion sequence of AI indicates the maximum near the volcano, suggests southward movement of the ash maximum over the hour, and shows a secondary lesser maximum (about 1° longitude southward) with a plume. TROPOMI, and thus ABI/TROPOMI fusion, also show cloud and land reflections that do not appear to be related to ash detection or the volcanic activity.

The difference in the dispersion of the volcanic SO_2 and the volcanic ash is evident when comparing the ABI/TROPOMI fusion images in Figures 4 and 5. ABI/TROPOMI SO_2 fusion shows a larger plume (likely because TROPOMI finds SO_2 more detectable than ash) with a secondary SO_2 maximum further away from

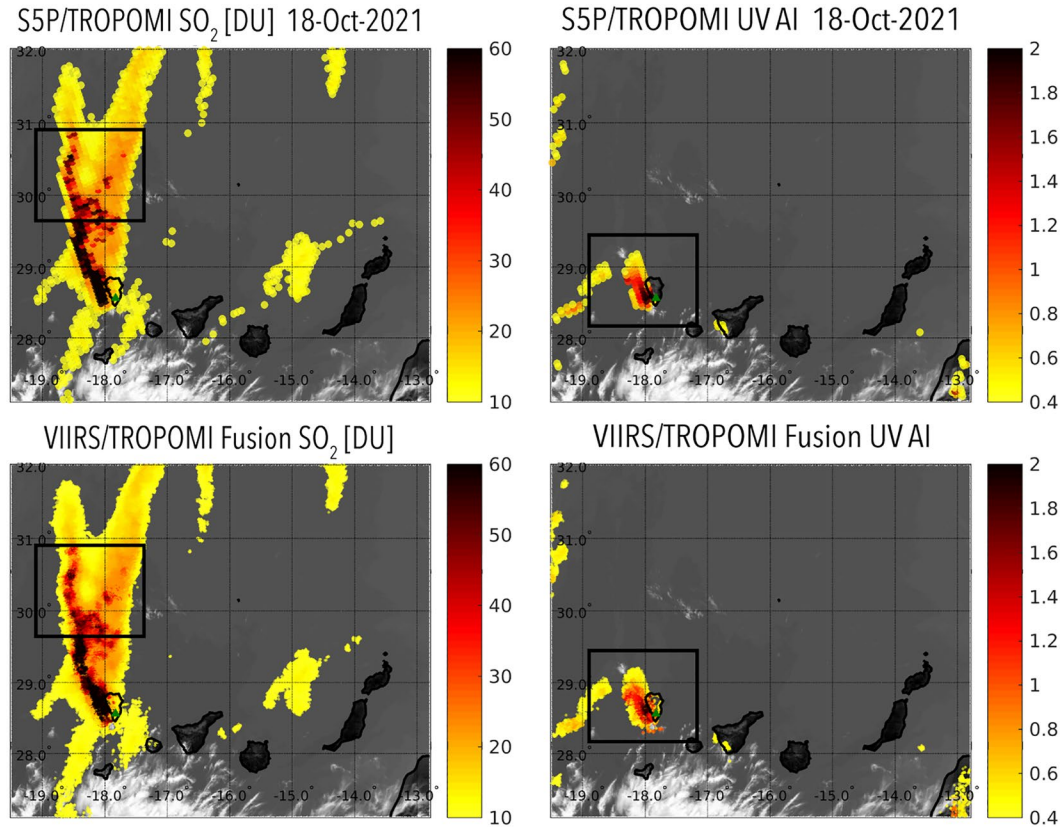

Figure 2. TROPOspheric Monitoring Instrument (TROPOMI) (top) and Visible Infrared Imaging Radiometer Suite (VIIRS)/TROPOMI fusion (bottom) of SO_2 in DU (left) and the UV AI (right), superimposed upon VIIRS Band 15 (10.7 μm) brightness temperatures for 18 October 2021. TROPOMI and NOAA-20 overpasses of La Palma occurred around 13:50 UTC and 14:30 UTC, respectively. The boxed area inside the panels is shown enlarged in Figure 3.

the volcano than the ABI/TROPOMI secondary ash maximum. The temporal fusion gives a sense of the SO_2 plume movement at high spatial resolution (2 km fusion versus 5.5 km TROPOMI) an hour before and after the TROPOMI overpass.

Ash and SO_2 may be separated (Schmidt et al., 2014; Stenchikov et al., 2021), horizontally and vertically, especially at some distance away from the volcano (and/or days after the eruption). It is important to note that airborne volcanic ash can be a serious hazard to aviation even hundreds of miles from an eruption (USGS Report, 2010), where it is often less detectable than SO_2, especially at night. Nighttime satellite-based infrared detection and tracking of SO_2 offers a possible indicator of the presence of volcanic ash (especially soon after volcanic emission) in the absence of a nighttime visible or NIR detection opportunity.

5. ABI/CrIS Fusion Results

As noted earlier, IASI with its continuous spectral sampling (in over IR 8,400 channels) is routinely used to provide accurate SO_2 total column and profile retrievals (Clarisse et al., 2008, 2012). IASI-derived SO_2 is often collocated with volcanic ash shortly after emission and may for sometimes thereafter indicate the presence of ash, but the dispersion of the concentrations of SO_2 and ash is highly variable (Sears et al., 2013). Furthermore, as mentioned above, ash and SO_2 are not always collocated, and ash, even in undetectable small amounts, is still considered to be a major threat to aviation (Carn et al., 2009). When viewed on radar, ash clouds do not always show up and cannot be seen at night. Space-borne high spectral resolution IR measurements offer a valuable nighttime complement to daytime SO_2 and ash detection from UV/VIS-NIR instruments such as TROPOMI.

To focus on the detection of SO_2 distribution on 18 October 2021, the ABI based k-d tree search is switched from the split-window BTD to the B10 (7.3 μm) radiances, since ABI B10 is sensitive to SO_2 absorption. Figure 6

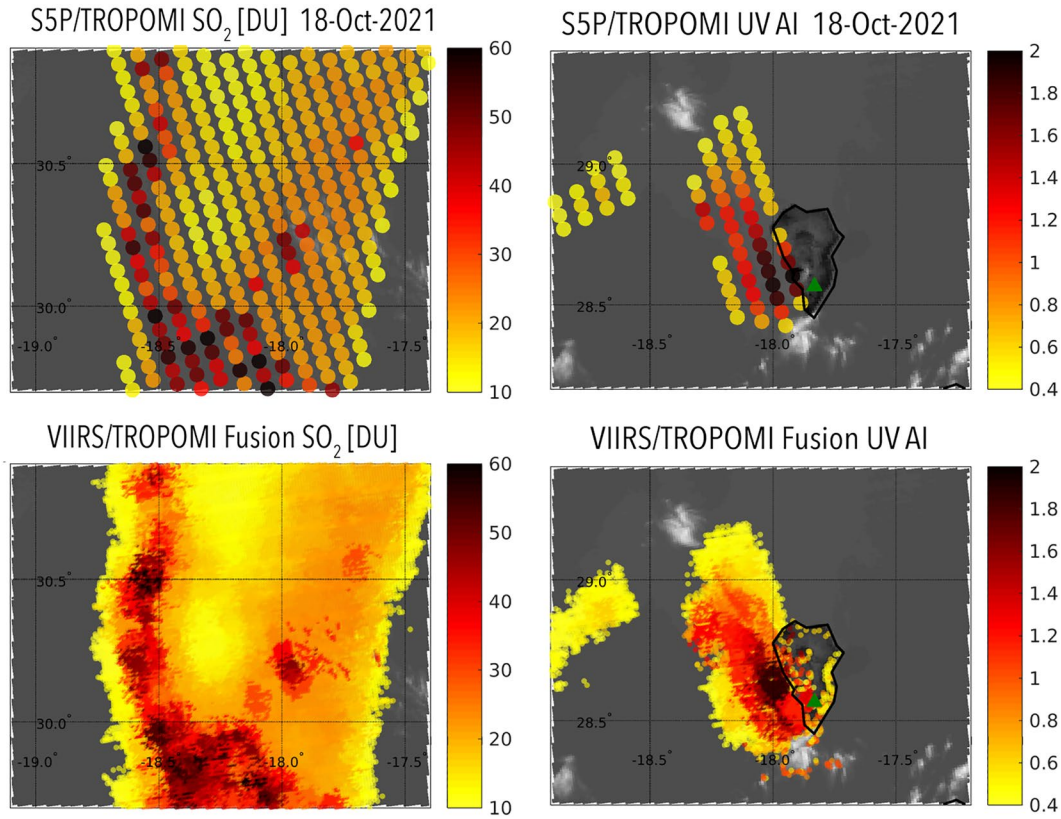

Figure 3. Zoomed in view of the boxed areas highlighted in Figure 2. TROPOspheric Monitoring Instrument (TROPOMI) (top) and Visible Infrared Imaging Radiometer Suite (VIIRS)/TROPOMI fusion (bottom) of SO_2 (left) and the UV AI (right), superimposed upon VIIRS Band 15 (10.7 μm) brightness temperatures for 18 October 2021.

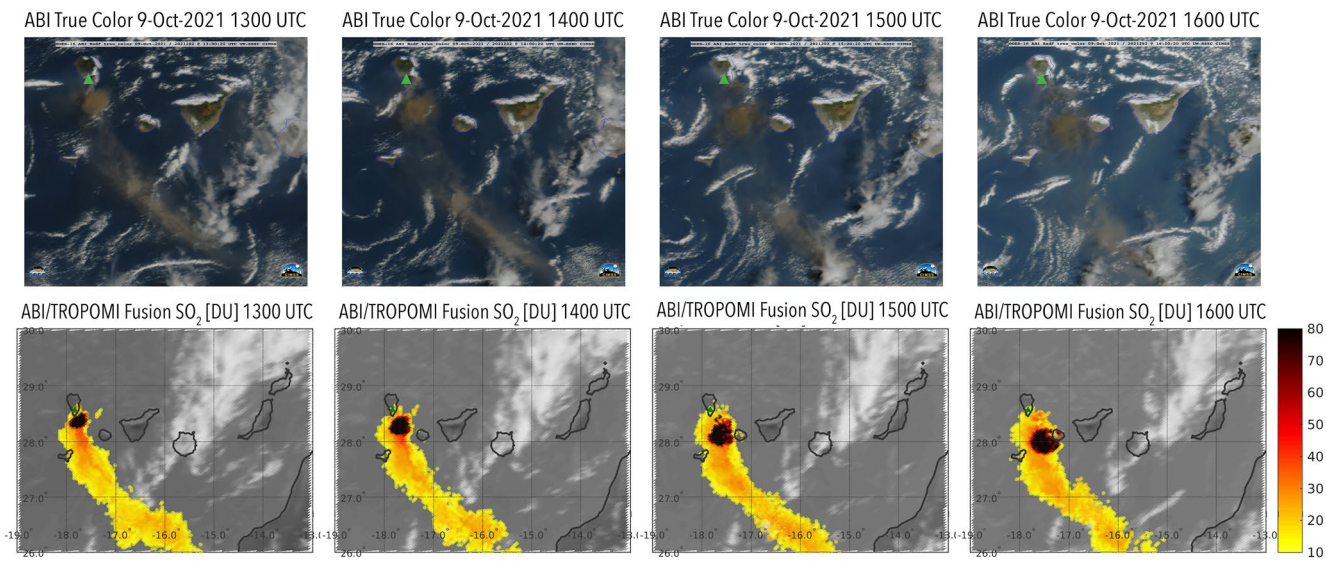

Figure 4. (Top) GOES-16 ABI True Color RGB images at 13:00, 14:00, 15:00, and 16:00 UTC on 9 October 2021. (Bottom) Advanced Baseline Imager/TROPOspheric Monitoring Instrument (ABI/TROPOMI) SO_2 fusion results in DU, superimposed upon ABI Band 13 (10.3 μm) brightness temperatures. Fusion starts at 15:00 UTC (i.e., the approximate time of the TROPOMI overpass), and works forward and backward in 10 min increments to produce the 13:00 to 16:00 UTC results.

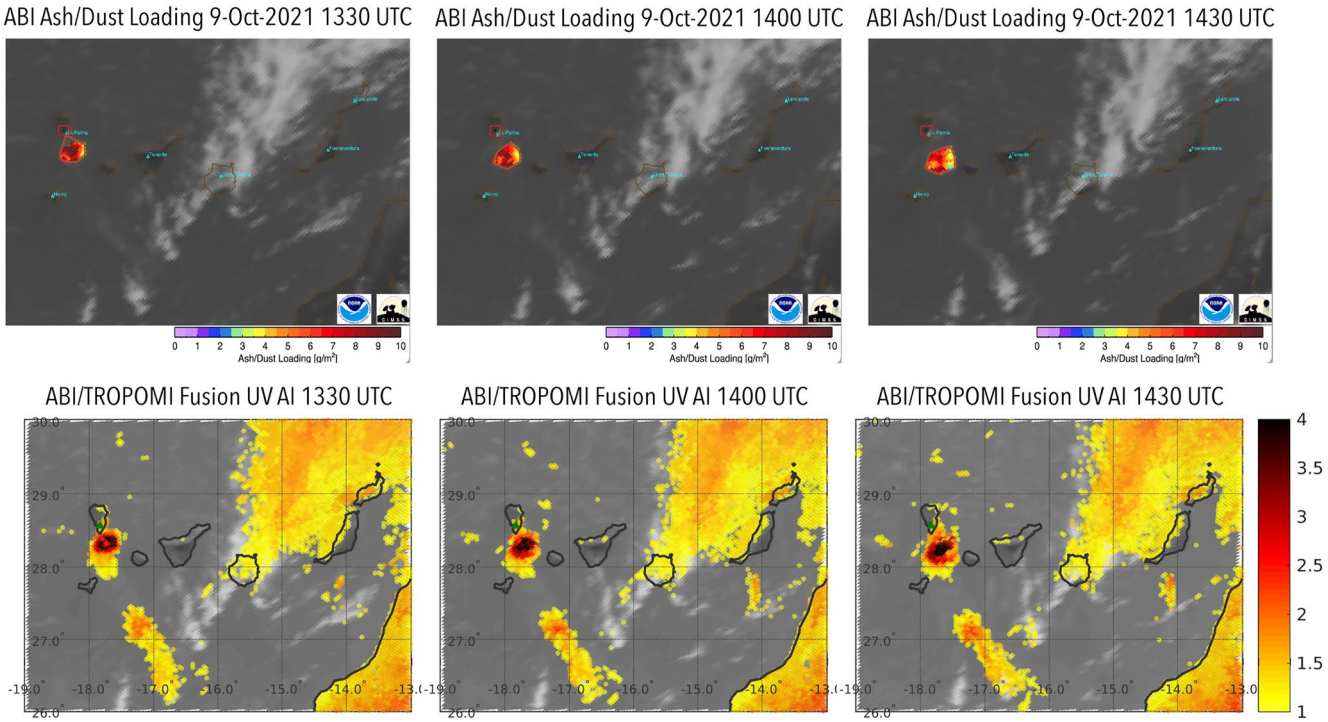

Figure 5. (Top) GOES-16 ABI Ash/Dust Loading in g/m^2 at 13:30, 14:00, and 14:30 UTC on 9 October 2021. (Bottom) ABI/TROPOspheric Monitoring Instrument UV AI fusion results, superimposed upon ABI Band 13 (10.3 μm). Fusion starts at 15:00 UTC and works backward in 10 min increments to produce the 13:30 to 14:30 UTC results.

shows a comparison of the ABI/TROPOMI fusion product when using the split-window BTD (middle panel of Figure 6) versus the SO_2-sensitive B10 radiances (right panel of Figure 6) in the k-d tree search; the fusion of the ABI/TROPOMI SO_2 products shows largely the same distribution in the zoom for the 18 October 2021 overpass. Comparison of the ABI/TROPOMI SO_2 product at 2 km resolution with the VIIRS/TROPOMI SO_2 fusion product at 750 m resolution (left panel of Figure 6 and also bottom left panel of Figure 3) again reveals the same distribution for pockets of SO_2 maxima. The correlation between the VIIRS/TROPOMI SO_2 fusion results (for roughly 18,500 VIIRS pixels) and the ABI/TROPOMI using the BTD search is 0.87, while for ABI/TROPOMI using the B10 radiance search it is 0.88. This lends confidence that the split-window BTD search has some skill in producing viable VIIRS/TROPOMI (VIIRS has no SO_2 sensitive infrared band) and ABI/TROPOMI fusion SO_2 products. It further shows that regardless of the instrument (VIIRS or ABI) used for the fusion, comparable results are obtained.

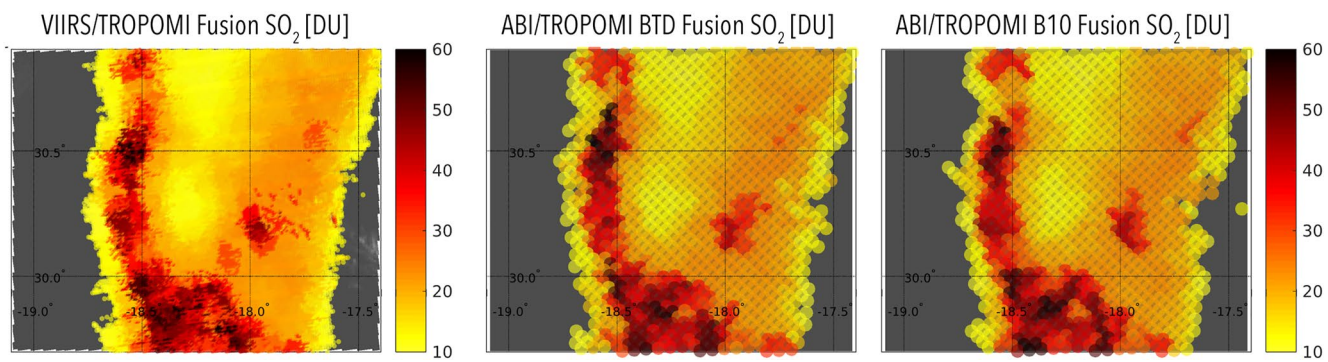

Figure 6. Zoomed in view (same as in Figure 3) of Visible Infrared Imaging Radiometer Suite/TROPOspheric Monitoring Instrument (VIIRS/TROPOMI) and two types of Advanced Baseline Imager (ABI)/TROPOMI fusion of SO_2 at 14:30 UTC (TROPOMI overpass time) on 18 October 2021. (Left) VIIRS/TROPOMI fusion using the VIIRS split-window in the k-d tree search (repeated from Figure 3 lower left). (Middle) ABI/TROPOMI fusion using the ABI split-window brightness temperature differences (BTD) in the k-d tree search; the correlation with the VIIRS/TROPOMI results is 0.87. (Right) ABI/TROPOMI fusion using the ABI B10 (7.3 μm) in the k-d tree search; the correlation with the VIIRS/TROPOMI results is 0.88.

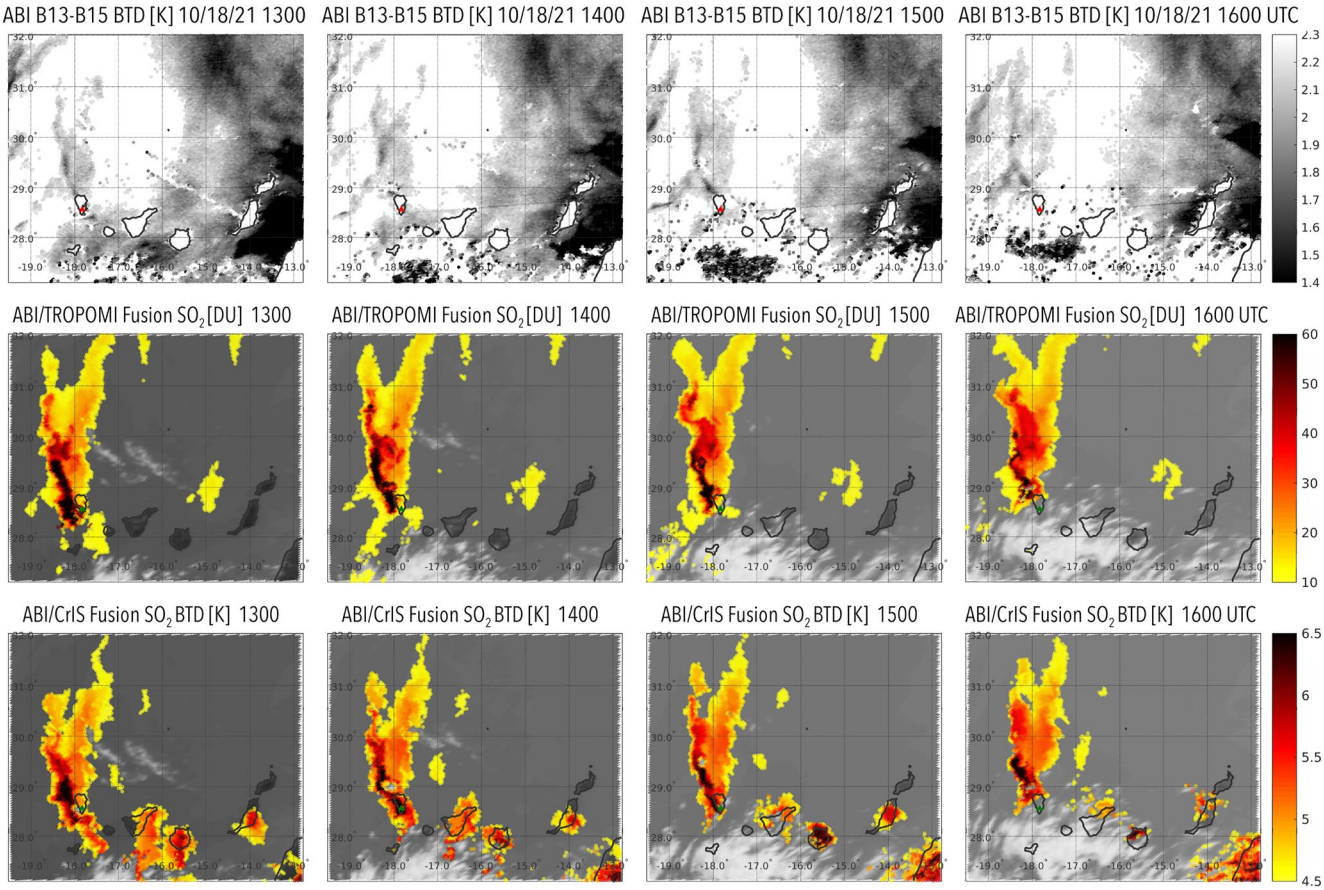

Figure 7. Advanced Baseline Imager (ABI) B13 (10.3 μm) minus B15 (12.3 μm) BT differences (top row), ABI/TROPOspheric Monitoring Instrument (TROPOMI) SO_2 fusion results in DU (middle row) and ABI/Cross-track Infrared Sounder (CrIS) BT differences (BTD) fusion for SO_2 (bottom row), in Kelvin (K) at 13:00, 14:00, 15:00, and 16:00 UTC on 18 October 2021. The fusion results are superimposed upon ABI Band 13 (10.3 μm). ABI/TROPOMI fusion (middle row) starts at 13:50 UTC and ABI/CrIS BTD fusion (bottom row) starts at 14:30 UTC, and both fusion types work forward and backward in 10 min increments to produce the 13:00 to 16:00 UTC results.

ABI fusion with NOAA-20 CrIS spectral measurements is now presented. The brightness temperature difference (BTD, given in degrees Kelvin or K) of wavenumbers 1,345 cm^{-1} (within the SO_2 absorption region) and 1,325 cm^{-1} (outside of the SO_2 absorption region) is calculated to determine the distribution and density of SO_2; when more SO_2 is detected the BTD increases (see Appendix A for more details). These infrared determinations are obtained both day and night.

In ABI/CrIS BTD fusion, the k-d tree search is performed with ABI B10 radiances, and then the associated CrIS BTD are averaged to yield new SO_2 sensitive BTDs with improved spatial resolution and temporal resolution. Figure 7 shows the comparison for 18 October 2021 of the ABI/TROPOMI fusion SO_2 (also performed with the ABI B10 radiance search) and the ABI/CrIS fusion SO_2 sensitive BT differences along with the ABI only BTD Band 13 minus Band 15 (10.3 μm minus 12.3 μm) indication of volcanic ash (Ackerman et al., 2008; Pavolonis et al., 2006; Prata & Kerkmann, 2007). TROPOMI shows spurious reflections not indicative of SO_2 in low clouds while CrIS has large BT differences issues over the nearby islands that are not caused by SO_2; ABI only split-window differences appear to be reliable in the vicinity of the volcano. For ABI/CrIS fusion (bottom row of Figure 7) the 14:30 UTC overpass of NOAA-20 CrIS BTD (shown in Figure 8 on the left) is transferred to earlier and later times, and the BTD changes in time are dictated by the ABI B10 changes through the fusion approach. We notice that ABI/CrIS fusion delineates much of the SO_2 dispersion found in ABI/TROPOMI fusion (middle row of Figure 7) while the ABI only split-window ash sensitive delineation (top row of Figure 7) is rather faint. ABI/CrIS BT differences 1,345 minus 1,325 cm^{-1} equal to 6 K or greater correlate with roughly ABI/TROPOMI indications of SO_2 concentrations of 60 DU or greater and ABI split-window temperature differences around 1.5 K. We find the hyperspectral measurements from sounders have more than twice (in this case four times) the

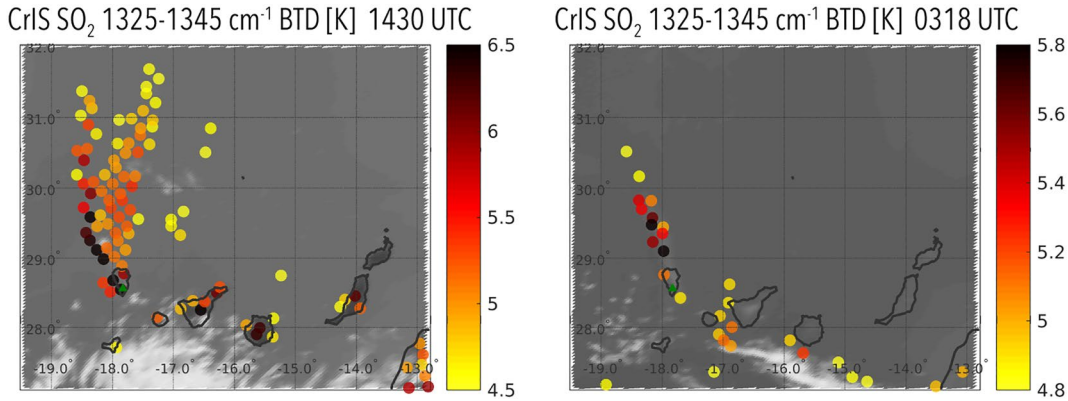

Figure 8. NOAA-20 CrIS SO_2 sensitive 1,325–1,345 cm^{-1} BT differences in K at 14:30 UTC (left) and 03:18 UTC (right) on 18 October 2021, superimposed upon ABI Band 13 (10.3 μm).

sensitivity to SO_2 than the broadband infrared measurements available from ABI, such as 10.3 μm minus 12.3 μm BTD (or 13.3 μm minus 7.3 μm BTD as discussed in Ackerman et al., 2008).

But CrIS as an IR instrument also has sensitivity to SO_2 at night. Figure 8 shows the CrIS detection of SO_2 from 18 October at 14:30 UTC (which has been used for the ABI/CrIS fusion results shown in Figure 7) along with the nighttime CrIS detection of SO_2 11 hr earlier at 03:18 UTC. The detection of the SO_2 plume is evident in the CrIS data both day and night, but again there is some unexplained detection of pockets of SO_2 over and near the islands east of La Palma.

Figure 9 shows a time series of the nighttime ABI/CrIS fusion results from 11 hr earlier; good delineation of the SO_2 plume location and the movement over 3 hr is evident. This illustrates the capability of CrIS for nighttime detection of SO_2 and of ABI/CrIS fusion to enhance the spatial and temporal depiction of the changes in the volcanic SO_2 plume at night. The plume is drifting eastward in the 3 hr of this loop; the ash movement is also shown in the ABI only split-window images (top row of Figure 9), but the extent of the ash plume is smaller. The SO_2 plume at night (Figure 9) on 18 October 2021 is found to expand during the subsequent day (Figure 7) suggesting further volcanic activity in the intervening hours.

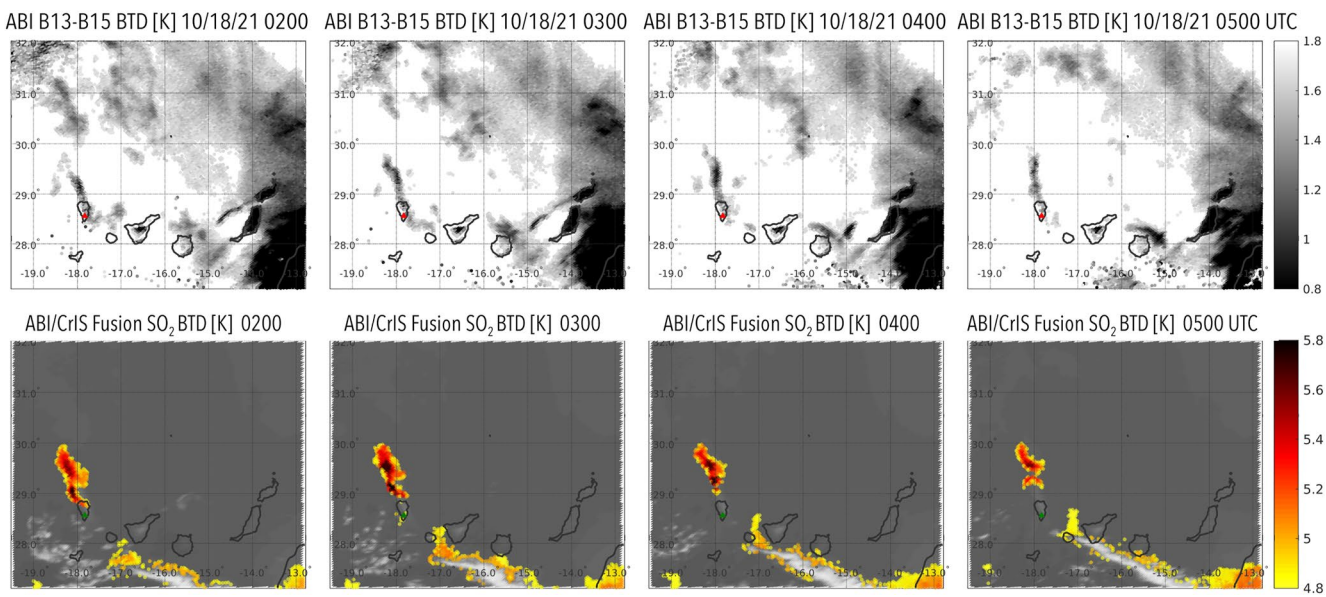

Figure 9. Advanced Baseline Imager (ABI) B13 (10.3 μm) minus B15 (12.3 μm) BT differences and ABI/Cross-track Infrared Sounder (CrIS) brightness temperature differences (BTD) fusion for SO_2 in K are shown in the top and bottom row, respectively, at 02:00, 03:00, 04:00, and 05:00 UTC on 18 October 2021. The fusion results are superimposed upon ABI Band 13 (10.3 μm). ABI/CrIS BTD fusion starts at 03:20 UTC and works forward and backward in 10 min increments to produce the 02:00 to 05:00 UTC results.

6. Summary and Conclusions

Fusion of TROPOMI detection of volcanic SO_2 and ash with infrared imager radiances of higher spatial resolution enables better delineation of the distribution of volcanic emissions. When the imager is hosted on a geostationary platform spatial fusion can be enhanced further by temporal fusion. Examples are shown for 2 days of VIIRS/TROPOMI and ABI/TROPOMI fusion of imager and sounder measurements over the Cumbre Vieja volcanic eruption. The synergy of GEO and LEO observations demonstrate the tracking of the SO_2 and ash in time sequences of the fusion products; this shows the potential for fusion to provide better definition and potential movement of the SO_2 as well as the ash. There is more sensitivity to SO_2 than ash in these satellite instrument measurements. Extension of the SO_2 detection into nighttime is demonstrated with IR CrIS measurements and ABI/CrIS fusion shows good potential both day and night.

The imager/sounder fusion approach to improve the volcanic gas and ash detection, presented here through three instrument pairings (VIIRS/TROPOMI, ABI/TROPOMI, and ABI/CrIS), has proven to be computationally efficient and stable. This allows the fusion product generation to be possible with real-time data, for example, in real-time trace gas monitoring systems. Real-time information on the presence of SO_2 and ash plumes (even days after and hundreds of miles away from the eruption center) is essential for implementation of accurate alert and warning systems that provide public and flight safety. Especially during nighttime, a better knowledge of the location of volcanic SO_2 where there is the potential for collocated ash can contribute to the improvement of aircraft safety procedures.

This work further provides an early indication of the anticipated impact of geostationary high spectral resolution sounders on trace gas monitoring and warning operations (and other applications) through an improved utility of LEO and GEO assets.

Appendix A: Infrared Spectral Selection for SO_2 Detection

The absorption band of SO_2 in the infrared centered around 1,360 cm^{-1} and extending from 1,320 to 1,400 cm^{-1} falls within the spectral region influenced by the vibrational and rotational lines of H_2O absorption centered around 1,550 cm^{-1} and extending from 1,340 to 2,000 cm^{-1}. Figure A1 shows a calculation of the brightness

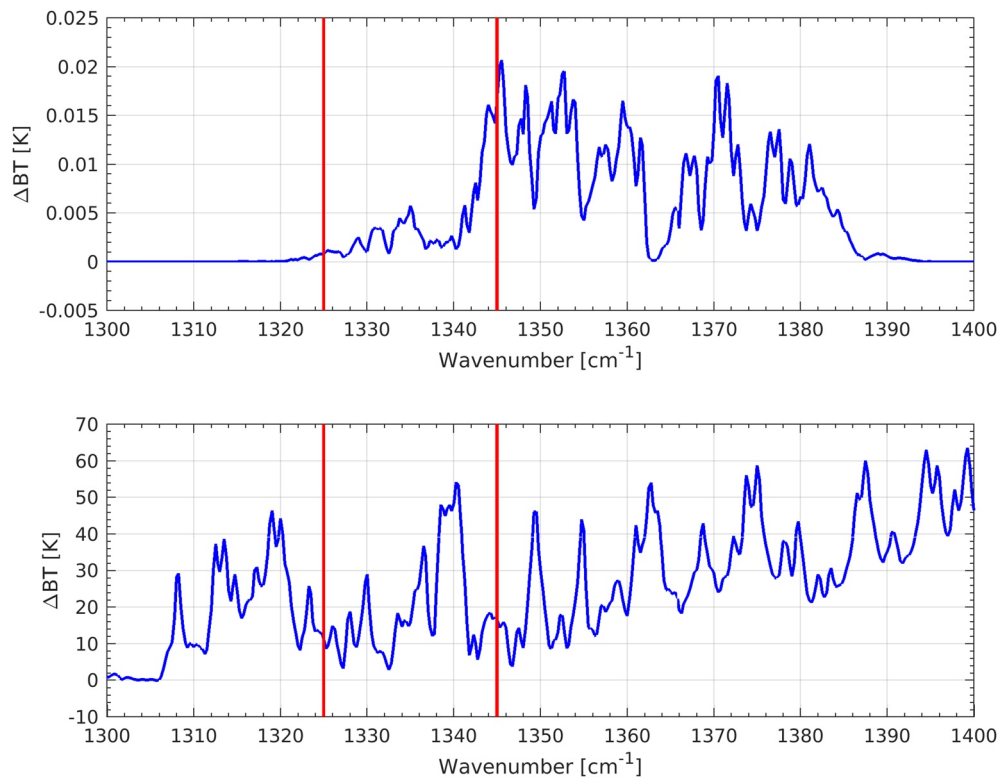

Figure A1. (Top) Simulated brightness temperature difference in the infrared spectrum from 1,320 to 1,400 wavenumbers for the US. standard atmosphere (1976) without sulfur dioxide (SO_2) minus with SO_2. (Bottom) Same for an atmosphere without H_2O minus with H_2O. Spectral locations of 1,325 and 1,345 cm^{-1} are highlighted in red.

temperature difference in a relevant portion of the earth-atmosphere emitted infrared spectrum in a standard mid latitude atmosphere that is caused by the removal of SO_2; it is accompanied by a similar calculation of the brightness temperature difference caused by the removal of H_2O. Selection of the spectral channels to highlight the effect of SO_2 must mitigate the effect of H_2O. The pairing of 1,325 cm^{-1} (not sensitive to SO_2) and 1,345 cm^{-1} (sensitive to SO_2), where both are equally sensitive to H_2O, makes the brightness temperatures 1,325 cm^{-1} minus 1,345 cm^{-1} capable of detecting and mapping the distribution of SO_2 (with the influence of H_2O canceled out in the difference). A similar approach using different spectral channels has been described in Clarisse et al. (2012).

Data Availability Statement

VIIRS, CrIS, and ABI Level 1 data, served as the input to the fusion algorithm in this study, can be accessed through the Atmosphere SIPS and the SSEC datacenter at the University of Wisconsin-Madison, Space Science and Engineering Center (SSEC) at https://sips.ssec.wisc.edu (VIIRS and CrIS L1, 2021) and https://www.ssec.wisc.edu/datacenter (GOES-16 ABI L1, 2021). Sentinel-5P TROPOMI data are available at the Sentinel-5P Pre-Operations Data Hub website https://s5phub.copernicus.eu/dhus/#/home (S5P TROPOMI, 2021), hosted by the European Space Agency (ESA). The GOES-16 ABI images (top rows of Figures 4 and 5) were extracted from animations found at https://cimss.ssec.wisc.edu/satellite-blog/archives/42806 (GOES-16 ABI Imagery, 2021), part of the UW-Madison/Cooperative Institute for Meteorological Satellite Studies (CIMSS) Satellite Blog. The imager plus sounder fusion algorithm used in this study is based on the VIIRS + CrIS radiance fusion approach as described by Weisz et al. (2017); the VIIRS + CrIS FSNRAD software package is described in Borbas et al. (2021).

Acknowledgments
The authors gratefully acknowledge the support from NASA and NOAA under Grant NA20NES4320003 and the encouragement of Dr. Daniel T. Lindsey (NOAA/NESDIS GOES-R Program Scientist). We acknowledge the usage of Sentinel-5P TROPOMI data from the ESA Copernicus Open Access Hub. We also thank the CIMSS satellite blog and the NOAA/CIMSS Volcanic Cloud Monitoring teams for the GOES-16 ABI images (shown in Figures 4 and 5).

References

Ackerman, S. A., Schreiner, A. J., Schmit, T. J., Woolf, H. M., Li, J., & Pavolonis, M. (2008). Using the GOES Sounder to monitor upper level SO_2 from volcanic eruptions. *Journal of Geophysical Research*, *113*, D14S11. https://doi.org/10.1029/2007JD009622

Baxter, P. (2005). Human impacts of volcanoes. In J. Martí, & G. G. J. Ernst (Eds.), *Volcanoes and the Environment* (pp. 273–303). Cambridge University Press. https://doi.org/10.1017/CBO9780511614767.011

Borbas, E., Weisz, E., Menzel, W. P., & Baum, B. A. (2021). Fusion of VIIRS and CrIS data to construct infrared (IR) absorption band radiances for VIIRS—Algorithm Theoretical Basis Document (ATBD). https://doi.org/10.5067/VIIRS/FSNRAD_L2_VIIRS_CRIS_SNPP.002

Carn, S. A., Clarisse, L., & Prata, A. J. (2016). Multi-decadal satellite measurements of global volcanic degassing. *Journal of Volcanology and Geothermal Research*, *311*, 99–134. https://doi.org/10.1016/j.jvolgeores.2016.01.002

Carn, S. A., Krueger, A. J., Krotkov, N. A., Yang, K., & Evans, K. (2009). Tracking volcanic sulfur dioxide clouds for aviation hazard mitigation. *Natural Hazards*, *51*(2), 325–343. https://doi.org/10.1007/s11069-008-9228-4

Carn, S. A., Newman, P. A., Aquila, V., Gonnermann, H., & Dufek, J. (2021). Anticipating climate impacts of major volcanic eruptions. *EOS—Science News by AGU*, *102*. https://doi.org/10.1029/2021EO162730

Clarisse, L., Coheur, P. F., Prata, A. J., Hurtmans, D., Razavi, A., Phulpin, T., et al. (2008). Tracking and quantifying volcanic SO_2 with IASI, the September 2007 eruption at Jebel at Tair. *Atmospheric Chemistry and Physics*, *8*(24), 7723–7734. https://doi.org/10.5194/acp-8-7723-2008

Clarisse, L., Hurtmans, D., Clerbaux, C., Hadji-Lazaro, J., Ngadi, Y., & Coheur, P.-F. (2012). Retrieval of sulphur dioxide from the infrared atmospheric sounding interferometer (IASI). *Atmospheric Measurement Techniques*, *5*(3), 581–594. https://doi.org/10.5194/amt-5-581-2012

Constantine, E. K., Bluth, G. J. S., & Rose, W. I. (2000). TOMS and AVHRR observations of drifting volcanic clouds from the August 1991 eruptions of Cerro Hudson. In P. J. Mouginis-Mark, J. A. Crisp, & J. H. Fink (Eds.), *Remote sensing of active volcanism. Geophysical Monograph* (Vol. 116, pp. 45–64). American Geophysical Union.

GOES-16 ABI Imagery (2021). GOES-16 ABI Level 1 and Level 2 imagery [Images]. UW-Madison/Cooperative Institute for Meteorological Satellite Studies (CIMSS) Satellite Blog archives. Retrieved from https://cimss.ssec.wisc.edu/satellite-blog/archives/42806

GOES-16 ABI L1 (2021). GOES-16 ABI Level 1 data [Dataset]. Online GOES Geostationary Archive at the Space Science and Engineering Center/University of Wisconsin-Madison. Retrieved from https://www.ssec.wisc.edu/datacenter/goes-archive/#GOES16

Han, Y., Revercomb, H., Cromp, M., Gu, D., Johnson, D., Mooney, D., et al. (2013). Suomi NPP CrIS measurements, sensor data record algorithm, calibration and validation activities, and record data quality. *Journal of Geophysical Research: Atmospheres*, *118*, 12734–12748. https://doi.org/10.1002/2013JD020344

Hillger, D., Kopp, T., Lee, T., Lindsey, D., Seaman, C., Miller, S., et al. (2013). First-light imagery from Suomi NPP VIIRS. *Bulletin of the American Meteorological Society*, *94*(7), 1019–1029. https://doi.org/10.1175/BAMS-D-12-00097.1

Karagulian, F., Clarisse, L., Clerbaux, C., Prata, A. J., Hurtmans, D., & Coheur, P. F. (2010). Detection of volcanic SO_2, ash, and H_2SO_4 using the infrared atmospheric sounding interferometer (IASI). *Journal of Geophysical Research*, *115*, D00L02. https://doi.org/10.1029/2009JD012786

López, R. P., & Jiménez, I. G. (2021). *The volcanic eruption of Cumbre Vieja in La Palma, 2021 [ConsorSeguros Revista Digital Number 15, Autumn 2021]*. Geological risk and climate change Dept. Spanish Geological Survey-Spanish National Research Council. Retrieved from https://www.consorsegurosdigital.com/en/numero-15/content/in-depth/the-volcanic-eruption-of-cumbre-vieja-in-la-palma-2021

Miller, S. D., Schmidt, C. C., Schmit, T. J., & Hillger, D. W. (2012). A case for natural colour imagery from geostationary satellites, and an approximation for the GOES-R ABI. *International Journal of Remote Sensing*, *33*(13), 3999–4028. https://doi.org/10.1080/01431161.2011.637529

Pavolonis, M., & Sieglaff, J. (2012). GOES-R advanced baseline imager (ABI) algorithm theoretical basis document for volcanic ash (detection and height), version 3 (30 July 2012). NOAA/NESDIS/STAR. Retrieved from https://www.star.nesdis.noaa.gov/goesr/documents/ATBDs/Baseline/ATBD_GOES-R_VolAsh_v3.0_July2012.pdf

Pavolonis, M. J., Feltz, W. F., Heidinger, A. K., & Gallina, G. M. (2006). A daytime complement to the reverse absorption technique for improved automated detection of volcanic ash. *Journal of Atmospheric Oceanic Technologies*, *23*(11), 1422–1444. https://doi.org/10.1175/JTECH1926.1

Poland, M. P., Lopez, T., Wright, R., & Pavolonis, M. J. (2020). Forecasting, detecting, and tracking volcanic eruptions from space. *Remote Sensing Earth System Sciences*, *3*(1–2), 55–94. https://doi.org/10.1007/s41976-020-00034-x

Prata, A. J. (2009). Satellite detection of hazardous volcanic clouds and the risk to global air traffic. *Natural Hazards*, *51*(2), 303–324. https://doi.org/10.1007/s11069-008-9273-z

Prata, A. J., & Kerkmann, J. (2007). Simultaneous retrieval of volcanic ash and SO_2 using MSG-SEVIRI measurements. *Geophysical Research Letters*, *34*, L05813. https://doi.org/10.1029/2006GL028691

Prata, A. J., & Tupper, A. (2009). Aviation hazards from volcanoes: The state of the science. *Natural Hazards*, *51*(2), 239–244. https://doi.org/10.1007/s11069-009-9415-y

Schmidt, A., Witham, C. S., Theys, N., Richards, N. A. D., Thordarson, T., Szpek, K., et al. (2014). Assessing hazards to aviation from sulfur dioxide emitted by explosive Icelandic eruptions. *Journal of Geophysical Research: Atmospheres*, *119*, 14180–14196. https://doi.org/10.1002/2014JD022070

Schmit, T. J., Griffith, P., Gunshor, M. M., Daniels, J. M., Goodman, S. J., & Lebair, W. J. (2017). A closer look at the ABI on the GOES-R series. *Bulletin of the American Meteorological Society*, *98*(4), 681–698. https://doi.org/10.1175/BAMS-D-15-00230.1

Sears, T. M., Thomas, G. E., Carboni, E., Smith, A. J. A., & Grainger, R. G. (2013). SO_2 as a possible proxy for volcanic ash in aviation hazard avoidance. *Journal of Geophysical Research: Atmospheres*, *118*, 5698–5709. https://doi.org/10.1002/jgrd.50505

Stein Zweers, D. C. (2021). *TROPOMI ATBD of the UV aerosol index (Doc. No. S5P-KNMI-L2-0008-RP)*. Royal Netherlands Meteorological Institute. Retrieved from https://sentinels.copernicus.eu/documents/247904/2476257/Sentinel-5P-TROPOMI-ATBD-UV-Aerosol-Index

Stenchikov, G., Ukhov, A., Osipov, S., Ahmadov, R., Grell, G., Cady-Pereira, K., et al. (2021). How does a Pinatubo-size volcanic cloud reach the middle stratosphere? *Journal of Geophysical Research: Atmospheres*, *126*, e2020JD033829. https://doi.org/10.1029/2020JD033829

S5P TROPOMI (2021). Sentinel-5 Precursor (S5P) TROPOMI (TROPOspheric Monitoring Instrument) trace gas Level 2 products [Dataset]. European Space Agency (ESA) Copernicus Sentinel-5 Precursor Pre-Operations Data Hub. Retrieved from https://s5phub.copernicus.eu/dhus/#/home

Theys, N., De Smedt, I., Lerot, C., Yu, H., & Van Roozendael, M. (2022). S5P/TROPOMI SO2 ATBD, BIRA-IASIB (Doc. No. S5PBIRA-L2-400E-ATBD). Retrieved from https://sentinels.copernicus.eu/documents/247904/2476257/Sentinel-5P-ATBD-SO2-TROPOMI

Theys, N., Hedelt, P., De Smedt, I., Lerot, C., Yu, H., Vlietinck, J., et al. (2019). Global monitoring of volcanic SO_2 degassing with unprecedented resolution from TROPOMI onboard Sentinel-5 Precursor. *Scientific Reports*, *9*(1), 2643. https://doi.org/10.1038/s41598-019-39279-y

USGS Report. (2010). *Reducing the risk from volcano hazards, airborne volcanic ash—A global threat to aviation*. U.S. Geological Survey. Retrieved from https://pubs.usgs.gov/fs/2010/3116/fs2010-3116.pdf

Veefkind, J. P., Aben, I., McMullan, K., Förster, H., de Vries, J., Otter, G., et al. (2012). TROPOMI on the ESA Sentinel-5 Precursor: A GMES mission for global observations of the atmospheric composition for climate air quality and ozone layer applications. *Remote Sensing of Environment*, *120*, 70–83. https://doi.org/10.1016/j.rse.2011.09.027

VIIRS and CrIS L1 (2021). VIIRS and CrIS Level 1 data [Datsaset]. NASA Atmosphere Science Investigator-led Processing Systems (SIPS), located at the Space Science and Engineering Center/University of Wisconsin-Madison. Retrieved from https://sips.ssec.wisc.edu/#/products/search

Weisz, E., Baum, B. A., & Menzel, W. P. (2017). Fusion of satellite-based imager and sounder data to construct supplementary high spatial resolution narrowband IR radiances. *Journal of Applied Remote Sensing*, *11*(3), 036022. https://doi.org/10.1117/1.JRS.11.036022

Weisz, E., & Menzel, W. P. (2019). Imager and sounder data fusion to generate sounder retrieval products at an improved spatial and temporal resolution. *Journal of Applied Remote Sensing*, *13*(3), 034506. https://doi.org/10.1117/1.JRS.13.034506

Weisz, E., & Menzel, W. P. (2020). Approach to enhance trace gas determinations through multi-satellite data fusion. *Journal of Applied Remote Sensing*, *14*(4), 044519. https://doi.org/10.1117/1.JRS.14.044519